nature nanotechnology

LETTERS

PUBLISHED ONLINE: 14 DECEMBER 2008 | DOI: 10.1038/NNANO.2008.369

Multimodal optical sensing and analyte specificity using single-walled carbon nanotubes

Daniel A. Heller[1], Hong Jin[1], Brittany M. Martinez[1†], Dhaval Patel[1†], Brigid M. Miller[1], Tsun-Kwan Yeung[1†], Prakrit V. Jena[2], Claudia Höbartner[3†], Taekjip Ha[2,4,5], Scott K. Silverman[3] and Michael S. Strano[1]*

Nanoscale sensing elements offer promise for single-molecule analyte detection in physically or biologically constrained environments. Single-walled carbon nanotubes have several advantages when used as optical sensors[1–3], such as photostable near-infrared emission for prolonged detection through biological media[2,4,5] and single-molecule sensitivity[6]. Molecular adsorption can be transduced into an optical signal by perturbing the electronic structure of the nanotubes[7]. Here, we show that a pair of single-walled nanotubes provides at least four modes that can be modulated to uniquely fingerprint agents by the degree to which they alter either the emission band intensity or wavelength. We validate this identification method *in vitro* by demonstrating the detection of six genotoxic analytes, including chemotherapeutic drugs and reactive oxygen species, which are spectroscopically differentiated into four distinct classes, and also demonstrate single-molecule sensitivity in detecting hydrogen peroxide. Finally, we detect and identify these analytes in real time within live 3T3 cells, demonstrating multiplexed optical detection from a nanoscale biosensor and the first label-free tool to optically discriminate between genotoxins.

Carbon nanotubes can be broadly functionalized and their one-dimensional electronic structure is sensitive to molecular adsorption. The mechanisms of signal transduction include charge-transfer interactions[1], which alter the Fermi level, and solvatochromic shifts[8], which modify intrinsic photoluminescence signatures, as we have shown[3]. The existence of multiple photoluminescent single-walled carbon nanotube (SWNT) species suggests untapped potential for multimodality, as variations in their responses can be used to discern molecular properties and identify analytes within a mixture. In this work, we make such a sensor defined by the differing responses of the (6,5) and (7,5) SWNT species. We detect and identify chemotherapeutic alkylating agents and reactive oxygen species (ROS) using the unique spectral responses generated by their interaction with DNA-encapsulated nanotubes.

Active alkylating drugs and ROS are important biological analytes that are difficult to measure *in vivo* or in real time[9]. Alkylating chemotherapeutic drugs from the nitrogen mustard and *cis*-platinum families are essential in treatments for many types of cancer. These drugs function by alkylating DNA, which leads to eventual strand breakage, resulting in apoptosis of mammalian cells[10,11]. The agents degrade in the body within a few hours, impeding their measurement in live cells and tissues. Standard techniques such as immunoassays, gel electrophoresis and nuclear magnetic resonance (NMR)[11,12] typically cannot be performed in live cells or require preparation steps that inhibit real-time measurement. Nucleic acid damage due to ROS interaction with DNA is widely suspected to have a role in oncogenesis and Alzheimer's disease[13–15]. Hydrogen peroxide, produced by mitochondria, reacts catalytically to produce several forms of ROS, including hydroxyl radicals, singlet oxygen and the superoxide anion[15,16]. These species, with half-lives of between a nanosecond and a millisecond in solution, form DNA adducts, crosslinks and strand breaks, but are difficult to observe because of their short lifetimes[15,17]. A label-free sensor that immediately converts chemical information into a near-infrared signal would be a promising tool for studying these challenging bioanalytes.

Figure 1a outlines four reaction pathways, which we measure by means of SWNT optical modulation. In the first reaction, the $d(GT)_{15}$ oligonucleotide-bound nanotube[18] (DNA–SWNT) is exposed to a chemotherapeutic alkylating agent (melphalan is shown), which reacts with the guanine nucleobase. This results in a uniform redshift in the photoluminescence bands of both (6,5) and (7,5) nanotubes (Fig. 1b). The second reaction shows direct adsorption of H_2O_2 by the nanotube, which results in attenuation of both the nanotubes' emission and a slight concomitant energy shift (Fig. 1c). Singlet oxygen, generated by exposing the nanotube complexes to Cu^{2+} and H_2O_2, causes a pronounced redshift of the (6,5) nanotube emission, but no corresponding shift in the (7,5) band (Fig. 1d). Finally, hydroxyl radicals, produced in the presence of SWNT by Fe^{2+} and H_2O_2, damage the DNA backbone and attenuate emission from both nanotubes but preferentially affect the (7,5) emission, without energy shifts (Fig. 1e). These spectral changes can be monitored transiently, allowing the dynamic behaviour of each agent to be elucidated as well as the clear differences between them (Fig. 1f–i). The same trends are evident upon varying genotoxin concentration (see Supplementary Information, Fig. S1).

Exposing DNA–SWNT to several analytes simultaneously achieves signal multiplexing. Concomitant generation of hydroxyl radicals and singlet oxygen elicits a precipitous initial intensity drop and pronounced (6,5) band intensity shifts, corresponding to the production of both analytes (see Supplementary Information, Fig. S2). Subsequent analysis, described below, confirms multiplexed detection.

[1]Department of Chemical Engineering, Massachusetts Institute of Technology, Cambridge, Massachusetts 02139, USA, [2]Department of Physics, University of Illinois at Urbana-Champaign, Urbana, Illinois 61801, USA, [3]Department of Chemistry, University of Illinois at Urbana-Champaign, Urbana, Illinois 61801, USA, [4]Beckman Institute for Advanced Science and Technology, University of Illinois at Urbana-Champaign, Urbana, Illinois 61801, USA, [5]Howard Hughes Medical Institute, Urbana, Illinois 61801, USA; †Present address: United States Patent and Trademark Office, Alexandria, Virginia 22314, USA (B.M.M.); School of Chemical and Biomolecular Engineering, Georgia Institute of Technology, Atlanta, Georgia 30332, USA (D.P.); Department of Physics, Harvard University, Cambridge, Massachusetts 02138, USA (T.-K.Y.); Max Planck Institute for Biophysical Chemistry, 37077 Göttingen, Germany (C.H.); *e-mail: strano@mit.edu

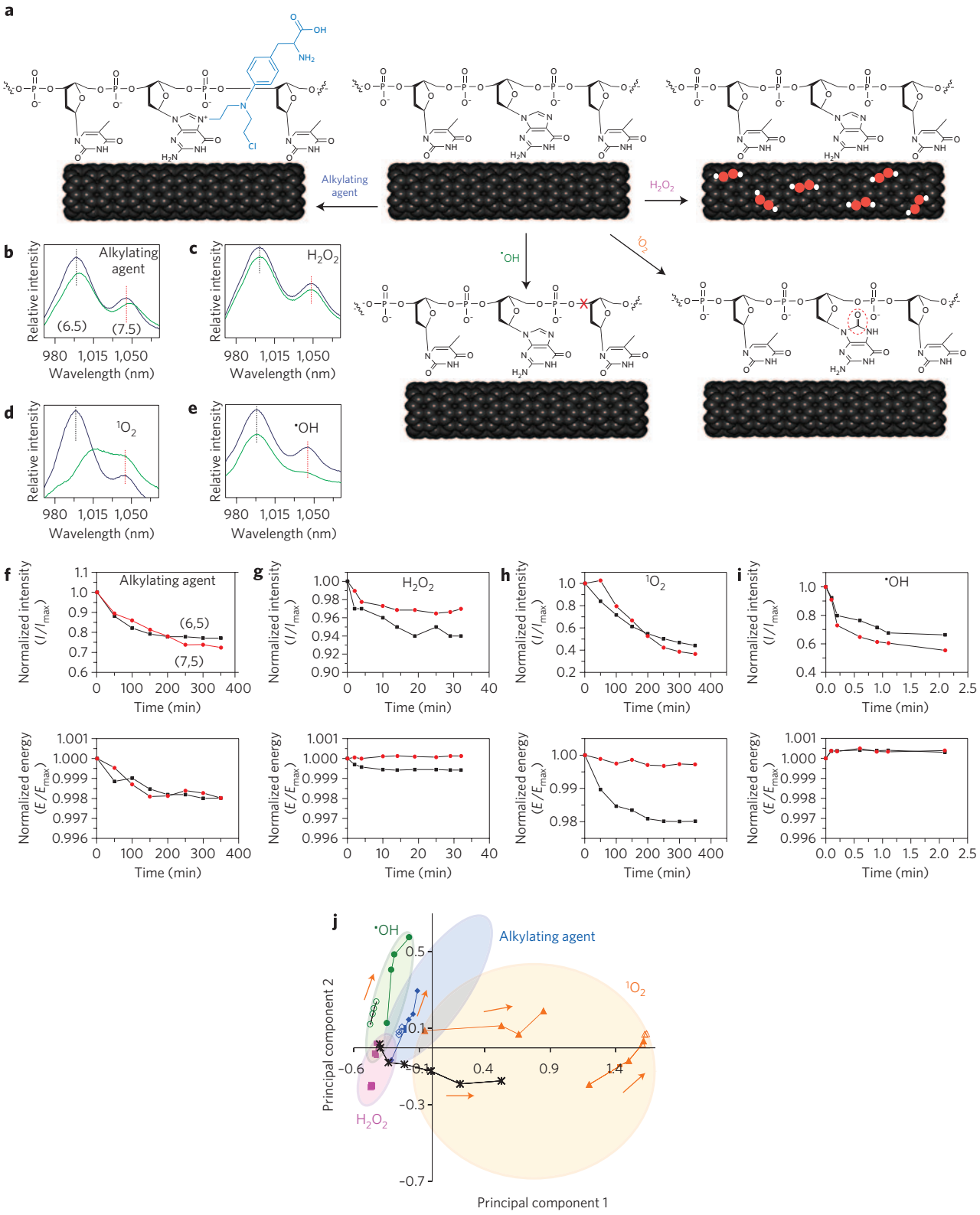

Figure 1 | Multimodal detection of four reaction pathways. a, Scheme of interactions on the DNA–SWNT complex—an alkylating agent reaction with guanine, H_2O_2 adsorption on the nanotube sidewall, a singlet oxygen ($^1O_2$) reaction with DNA, and hydroxyl radical (•OH) damage to DNA. **b**–**e**, DNA–SWNT photoluminescence spectra before (blue) and after (green) introducing mechlorethamine (**b**), H_2O_2 (**c**), singlet oxygen (**d**) and hydroxyl radicals (**e**). **f**–**i**, Transient responses of photoluminescence intensity (top panels) and energy (bottom panels) of the (6,5) nanotube (black) and (7,5) nanotube (red) upon introducing mechlorethamine (**f**), H_2O_2 (**g**), singlet oxygen (**h**) and hydroxyl radicals (**i**). **j**, Plot of first two principal component scores of transient (filled symbols) and concentration-dependent (open symbols) detection data (from Supplementary Information, Fig. S1). Black crosses represent simultaneous singlet oxygen and hydroxyl radical generation (from Supplementary Information, Fig. S2b). Area-minimized ovals encompass all data sets taken for each analyte, including those not shown. Arrows denote directions of increasing concentration or time.

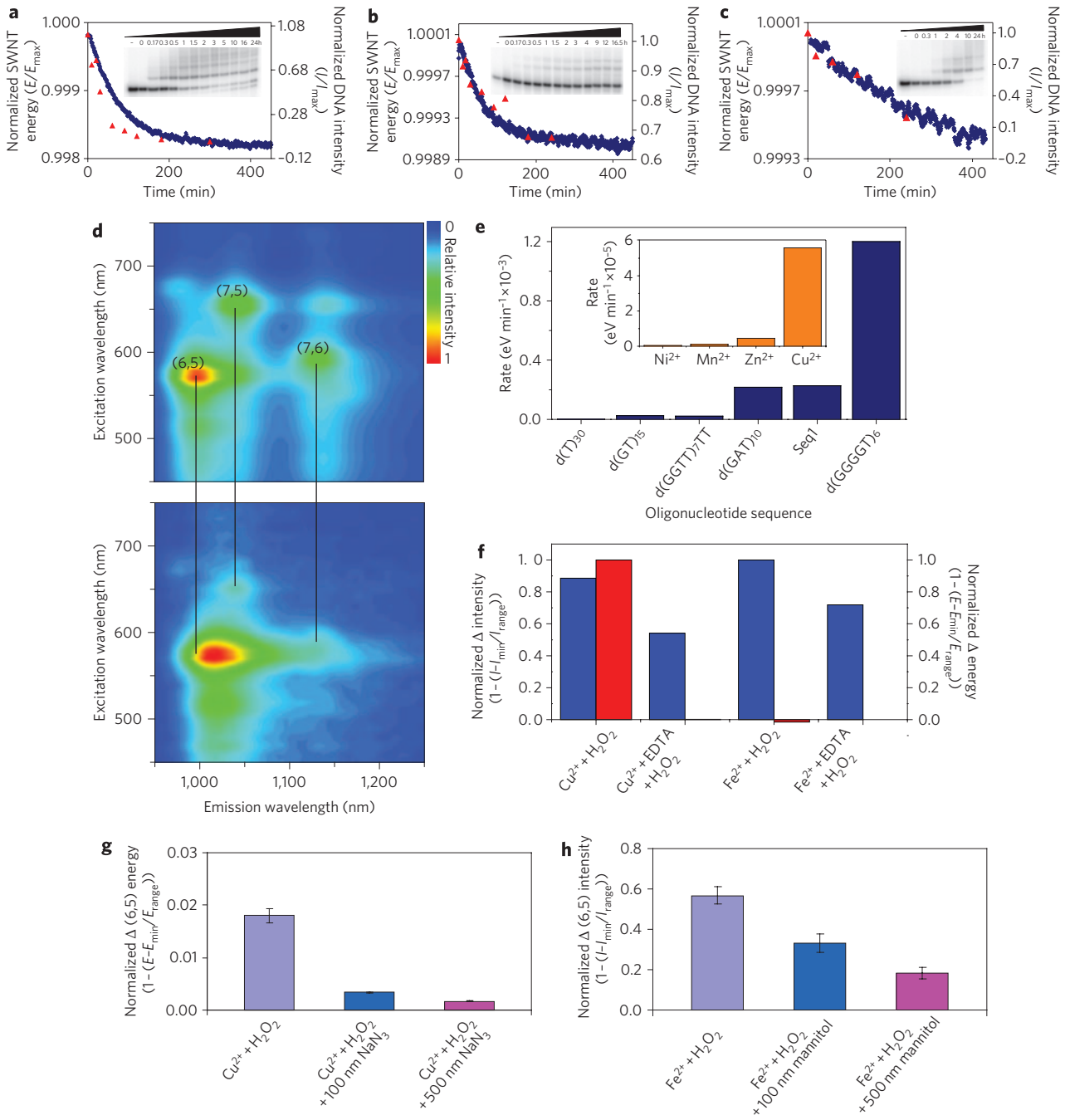

Figure 2 | Mechanistic studies of SWNT–genotoxin reactions. a, Photoluminescence shift of the (6,5) nanotube (blue curve) upon DNA–SWNT exposure to melphalan and a kinetics trace of unreacted oligonucleotide band intensity (red curve) from 20% PAGE (inset) upon melphalan-induced alkylation of an unbound test sequence. **b**, The same data for the mechlorethamine-induced response. **c**, The same data for the cisplatin response. **d**, 3D photoluminescence profiles of DNA–SWNT before (top) and after (bottom) inducing singlet oxygen generation. **e**, Rate of singlet oxygen-induced (6,5) band redshifting of SWNT encapsuled by oligonucleotide sequences of increasing purinic character (from left to right; see Methods for Seq 1—67% purines). Inset: The rate of (6,5) band redshift induced by singlet oxygen generated by H_2O_2 and cations with increasing nucleobase-binding capability (from left to right) on $d(GT)_{15}$ encapsulated SWNT. **f**, Chelation of Cu^{2+} with EDTA prevents all (6,5) peak shifting (red) upon the introduction of H_2O_2. Chelating either Fe^{2+} or Cu^{2+} reduces (6,5) signal attenuation (blue) upon introducing H_2O_2. **g**, Sodium azide diminishes (6,5) nanotube energy shift triggered by Cu^{2+}/H_2O_2. **h**, Mannitol reduces Fe^{2+}/H_2O_2 induced signal attenuation. Error bars in **g**,**h** denote standard deviation.

Principal components analysis[19] (PCA) validates analyte fingerprinting. The subspace determined by the first two principal component scores (see Methods section for details) of all transient and concentration-dependent (6,5) and (7,5) response data exhibits segregation by analyte (Fig. 1j). (PCA scores are listed in the Supplementary Information, Table S1.) This confirms analyte identification based on the four signal transduction modes. Analysis of simultaneous reagent detection (see Supplementary Information, Fig. S2) verifies multiplexed detection, as early time points cluster in the hydroxyl radical and H_2O_2 zones, and later points locate in the singlet oxygen region. We investigated the nature of all analyte responses as described below.

Chemotherapeutic alkylating agents are detected immediately upon exposure to the DNA–SWNT complex. Emission redshifts of

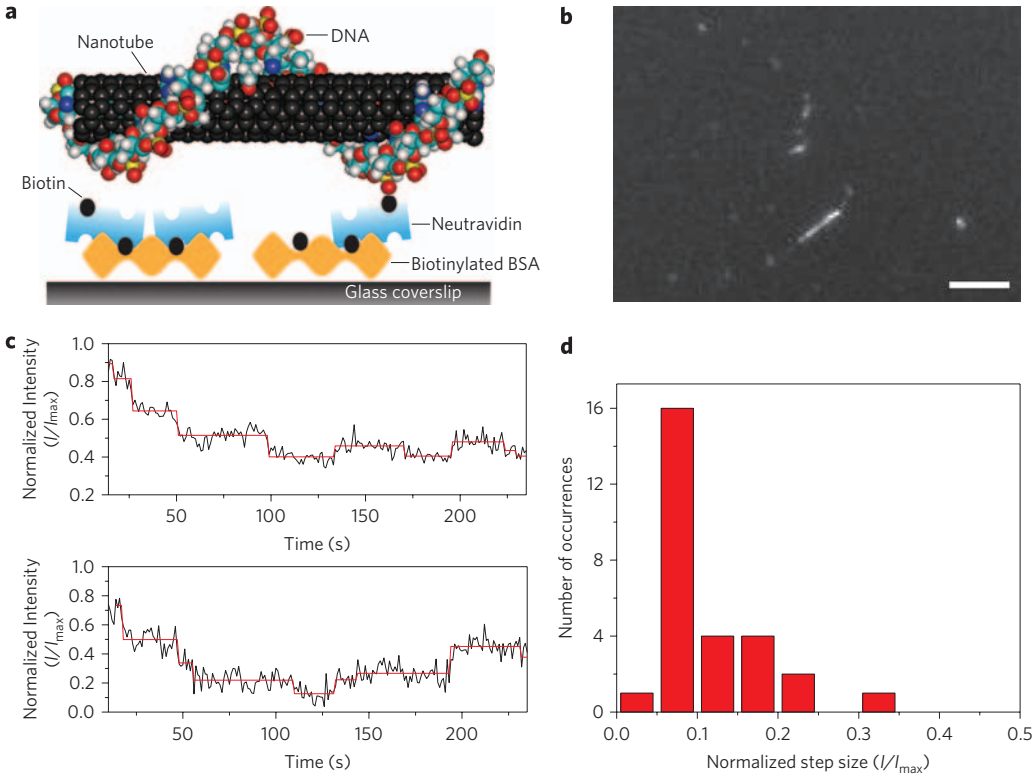

Figure 3 | Single-molecule H_2O_2 detection. a, Schematic of biotinylated DNA–SWNT binding to a glass surface with BSA–biotin and Neutravidin. **b**, Single near-infrared movie frame showing photoluminescence from several DNA–SWNT complexes (scale bar, 10 μm). **c**, Fitted traces from a movie showing single-step SWNT emission quenching upon perfusion of H_2O_2. **d**, Histogram of fitted step sizes from five traces taken from one near-infrared movie.

up to 6 meV and concomitant attenuation were observed using near-infrared spectrofluorimetry (Fig. 2a–c; see also Supplementary Information, Fig. S3). The redshifting rates caused by the nitrogen mustards melphalan and mechlorethamine are similar (first-order $k_{obs} = 0.014$ min^{-1} and 0.012 min^{-1}, respectively), whereas cisplatin promotes a threefold lower shift rate ($k_{obs} = 0.0047$ min^{-1}). The rate of drug alkylation to an unbound test oligonucleotide containing one guanine nucleobase, analysed by polyacrylamide gel electrophoresis, is similar to the rate of drug-induced DNA–SWNT shift ($k_{obs} = 0.0083$ min^{-1} for mechlorethamine and $k_{obs} = 0.0058$ min^{-1} for cisplatin; direct comparison to $d(GT)_{15}$ is provided in the Supplementary Information, Fig. S4). The DNA–SWNT response of melphalan is slower than the unbound DNA alkylation ($k_{obs} = 0.028$ min^{-1}), which we attribute to the steric bulk of this larger molecule as it interacts with the nanotube-bound DNA. The rates of SWNT emission shifting are highly sequence-dependent, proportional to the abundance of guanine in the bound oligonucleotide sequence (see Supplementary Information, Fig. S5), which is consistent with the known preference of melphalan for alkylating purine nucleobases[10]. We conclude that the DNA–SWNT complex emission responds to the alkylation of the bound oligonucleotide by means of a solvatochromic shift mechanism[8] due to the introduction of the drug adduct into the immediate vicinity of the nanotube, resulting in conformational changes of the encapsulating DNA.

Hydrogen peroxide is detected by the DNA–SWNT complex through attenuation of both (6,5) and (7,5) fluorescence bands to similar extents with slight shifting of peak wavelengths (Fig. 1c). Reversible charge-transfer quenching upon H_2O_2–SWNT contact, caused by peroxide's high reduction potential, is responsible for this behaviour[20]. Although (6,5) and (7,5) nanotube signals show similar attenuation in this study, small-bandgap nanotubes attenuate to a greater extent, in agreement with absorption spectroscopy studies[21] (data are provided in the Supplementary Information, Fig. S6). This provides an additional basis for fingerprinting H_2O_2 for studies involving small-bandgap SWNT species.

Singlet oxygen formed in the direct vicinity of the DNA–nanotube complex induces a pronounced redshift in (6,5) nanotube emission with virtually no (7,5) nanotube shift (Fig. 1d), as confirmed by the three-dimensional photoluminescence profile (Fig. 2d). Shifts of over 60 meV (50 nm) have been observed, as well as small red- and blueshifts of other SWNT species along with relative attenuation of large-bandgap species (see Supplementary Information, Fig. S7). Similar trends are seen in absorption spectra (see Supplementary Information, Fig. S8). The effect of singlet oxygen on the DNA–SWNT signal is sequence-dependent, as various strands used to encapsulate the nanotube in place of $d(GT)_{15}$ promote shift rates roughly proportional to the abundance of purine nucleobases in the sequence (Fig. 2e); purines are the most easily oxidized nucleobases[22]. The rate measured among several metal ion catalysts (Fig. 2e, inset) is greater for ions that demonstrate higher binding affinity to nucleobases[23], suggesting that singlet oxygen causes the redshift when produced in the vicinity of the nucleobases. By preventing singlet oxygen generation in the nanotube's immediate vicinity, by chelating all available Cu^{2+} ions with EDTA[24], the wavelength shift is completely inhibited and signal attenuation is reduced (Fig. 2f). Exposure to the singlet oxygen scavenger sodium azide significantly reduces the magnitude of the (6,5) band shift (Fig. 2 g); however, its introduction after shifting does not cause a reversal. These experiments suggest that this unique SWNT response is due to a singlet oxygen-induced DNA adduct resulting from nucleobase oxidation, such as 8-oxo-deoxyguanosine[25]. The oxidized nucleobase increases the polarity of the nanotube's microenvironment, causing a

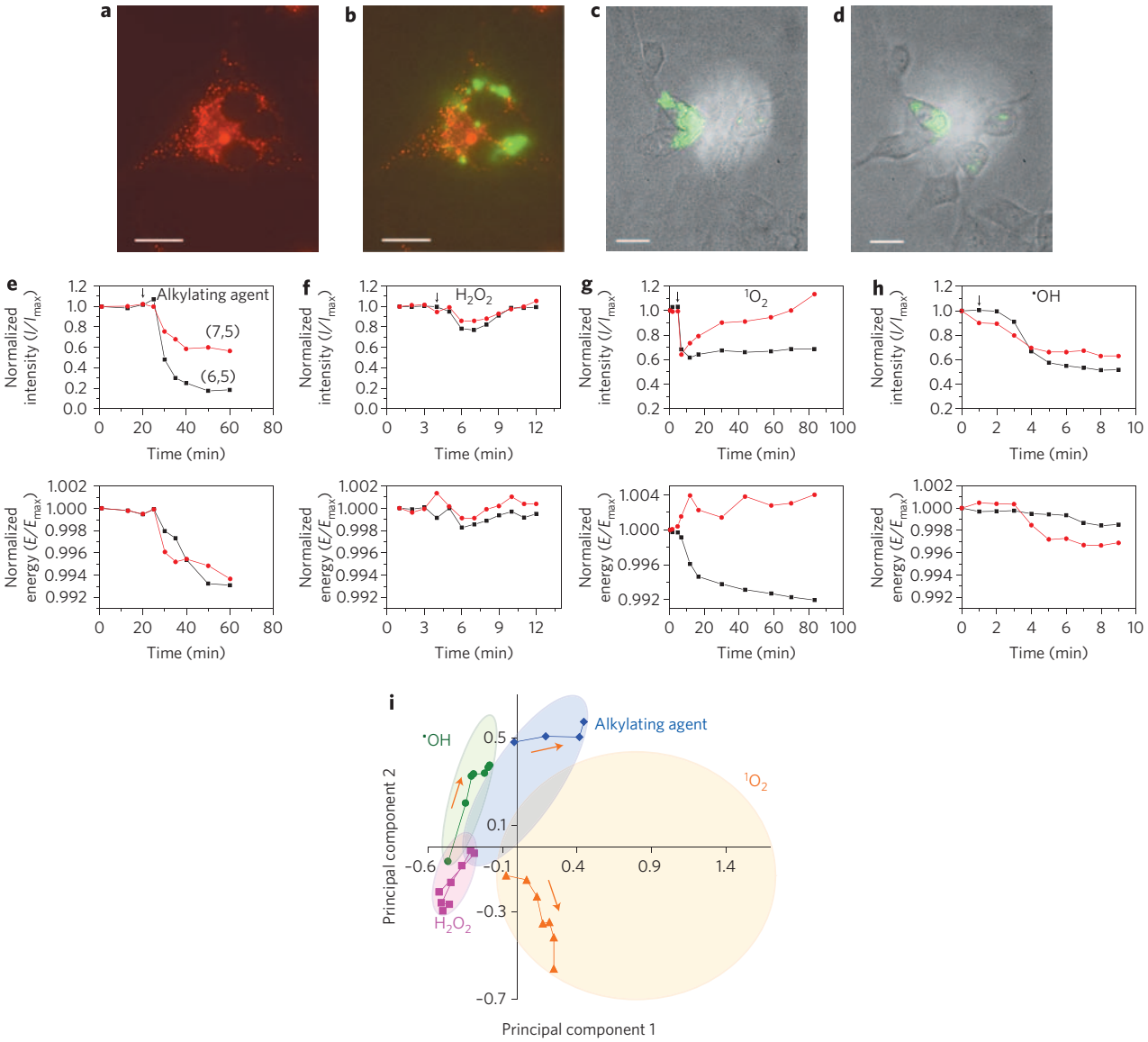

Figure 4 | Real-time multiplexed detection of genotoxins in live mammalian cells. a, Fluorescence of lysosomal stain Lysotracker in 3T3 cells. **b**, DNA–SWNT photoluminescence (green) showing partial co-localization with Lysotracker emission. **c**,**d**, Photoluminescence of DNA–SWNT (green) overlaying visible 3T3 cell images (grey) in the presence of Fe^{2+} before (**c**) and after (**d**) introduction of H_2O_2. (Scale bars in **a**–**d**, 20 μm.) **e**–**h**, Photoluminescence intensity (top panels) and energy (bottom panels) of the (6,5) nanotube (black trace) and (7,5) nanotube (red trace) after introducing mechlorethamine (**e**), H_2O_2 (**f**), singlet oxygen (**g**) and hydroxyl radicals (**h**). Arrows denote the time of agent addition. **i**, Principal components analysis of *in vivo* data showing segregation of data into discrete regions. Area-minimized ovals encompass regions defined by all available data for each analyte. Arrows denote direction of increasing time.

solvatochromic redshift. Response variations between nanotubes result from SWNT structural and electronic differences, which cause DNA–nanotube interactions to vary across species, resulting in diverse responses to DNA adduct formation. Identification of the dominant adduct formed in this case will be the focus of future work.

Generation of the hydroxyl radical by the Fenton reaction[15] is detected by the DNA–SWNT complex through attenuation of the photoluminescence from the nanotubes. The Fe^{2+} ion catalyses hydroxyl radical formation in the presence of H_2O_2, which, in the vicinity of DNA–SWNT, greatly attenuates both (6,5) and (7,5) fluorescence bands without shifting the peak wavelengths and generally attenuates the (7,5) nanotube emission to a greater extent (Fig. 1e). Chelation of all available Fe^{2+} with EDTA reduces, but does not eliminate, signal attenuation, suggesting that damage can be detected without close association of Fe^{2+} to the nucleobases (Fig. 2f). Mannitol, a hydroxyl radical quencher[25], prevents signal attenuation when added before initiating the reaction (Fig. 2 h). Hydroxyl radical interaction with DNA–SWNT exhibits highly disproportional attenuation of small-bandgap species emission (see Supplementary Information, Fig. S9). We thus conclude that the DNA–SWNT complex detects the hydroxyl radical by induced DNA damage. The resulting DNA adduct includes a species that induces photoluminescence attenuation by a charge-transfer mechanism.

Stepwise near-infrared photoluminescence quenching of surface-tethered DNA–SWNT complexes demonstrates single-molecule detection of H_2O_2. Recent work has shown that analyte–SWNT interactions can be studied at the single-molecule level through immobilization of surfactant-suspended nanotubes in agarose[6]. We encapsulated nanotubes with a 1:4 ratio of biotinylated to nonbiotinylated $d(GT)_{15}$, allowing Neutravidin-specific binding

of DNA–SWNT to a BSA–biotin treated surface (Fig. 3a) (see Supplementary Information for methods). Immobilized DNA–SWNT complexes were imaged using their near-infrared photoluminescence signal upon laser excitation (Fig. 3b). Time traces of SWNT quenching (Fig. 3c) were obtained by measuring the intensity of four-pixel spots in movies recorded at 1 frame per second, resulting in multiple traces that exhibit single-step attenuation upon perfusion of H_2O_2. The traces yield a narrow histogram of normalized quantized intensity changes after regression with a stochastic step-fitting algorithm[26], confirming the discrete nature of the interaction (Fig. 3d). The average normalized step height of 0.05–0.1 is consistent with a 90-nm exciton excursion range[6] and spot size of 900 nm, confirming a quantized single-step magnitude of 0.1. These measurements demonstrate single-molecule detection of H_2O_2, providing promise for new classes of biosensors with this level of sensitivity.

Nucleic acid encapsulated SWNTs enter cells through endocytosis, without exhibiting cytotoxic effects at doses of at least 5 mg l^{-1} (ref. 27) while maintaining their photoluminescence properties[28,29], which can be perturbed *in situ*[3]. Co-localization images of nanotube fluorescence in murine 3T3 cells with a lysosomal stain show partial overlap, suggesting DNA–SWNT presence in both lysosomes and the cytoplasm (Fig. 4a,b). Perfused chemotherapeutic drugs and ROS induce SWNT spectral changes in real time within live cells, allowing detection *in situ* using this multimodal technique. The photoluminescence intensity changes of DNA–SWNT, upon interaction with genotoxins, can be spatially resolved within single cells, as shown in images before and after inducing hydroxyl radical formation (Fig. 4c,d).

Four genotoxins have been demonstrably detected and identified in live cells spectroscopically. Real-time measurements reveal that the alkylating agent mechlorethamine induces a detectable attenuation and peak shift of both (6,5) and (7,5) nanotube bands following perfusion of the drug into cell media, similar to *in vitro* behaviour (Fig. 4e). Perfusion with H_2O_2 alone induces a temporary attenuation of both nanotube bands, with minimal shifting, that reverses within 5 to 10 minutes (Fig. 4f). The reversibility is expected due to the cellular enzymes that decompose H_2O_2 (ref. 30). Movies of SWNT emission in cells elucidate spatially heterogeneous quenching observed upon H_2O_2 perfusion (see Supplementary Information, Fig. S10 and Video). Singlet oxygen (Fig. 4g) and hydroxyl radicals (Fig. 4h), generated *in vivo* by perfusion of their respective catalytic reagents, produce trends generally consistent with the DNA–SWNT response *in vitro*, although the intensities exhibit some deviation. Such events are expected during detection in single cells, as cell movement can cause intensity fluctuations. Additionally, endosomal localization and the DNA coating may lower the detection limit due to aggregation caused by endosome fusion and protein binding to DNA–SWNT[29,31]. Analysis using PCA reveals that cellular responses uniquely fingerprint each genotoxin. A principal components plot (Fig. 4i) shows analyte data separated into distinct regions, consistent with *in vitro* data (Fig. 1j).

In conclusion, we report that single-walled carbon nanotubes can act as a unique multimodal sensor for separate reaction pathways and biologically relevant analytes. The findings introduce new spectral phenomena previously unknown in carbon nanotubes. Moreover, the work demonstrates the first multiplexed optical detection from a nanoscale sensor and provides the first tool to identify and measure both alkylating and ROS activity in real time within living cells. The specificity and versatility of detection suggest significant and numerous diagnostic and metrologic applications for this approach.

Methods

SWNT preparation. Raw HiPCO SWNTs (Rice University) were suspended using bath sonication for 1 h in a 1:1 mass ratio with the $d(GT)_{15}$ oligonucleotide. The resulting solution was centrifuged at 16,300*g* for 90 min and the pellet discarded. Raw CoMoCAT SWNTs (Southwest Nanotechnologies) were suspended using probe-tip sonication at 10 W for 10 min in a 4:1 ratio with $d(GT)_{15}$ in 0.1 M NaCl cooled by an ice bath. The resulting GT–CoMoCAT solution was centrifuged at 16,300*g* for 90 min and the pellet discarded.

Spectroscopy and microscopy. Near-infrared photoluminescence spectra were acquired using 785 nm excitation and an Acton SP-150 spectrograph coupled to a Princeton Instruments OMA V InGaAs detector or with a Kaiser Holospec f/1.8 Imaging Spectrograph (Kaiser Optical). Absorption measurements were taken with a Shimadzu UV-3101 PC UV-VIS-NIR scanning spectrophotometer. Photoluminescence three-dimensional profiles were acquired with an in-house built spectrofluorometer incorporating a xenon arc lamp, Kratos GM-252 monochromators and an E1-L Germanium Detector (Edinburgh Instruments). Single-molecule and cell microscopy studies used a Carl Zeiss Axiovert 200 fluorescence microscope coupled to a Princeton Instruments 2D-OMA V InGaAs camera with a 256 × 320 pixel array and Acton spectrograph. Visible fluorescence images were acquired with an AxioCam MRm CCD camera. Spectra were processed by fitting to a Gaussian lineshape to determine the peak centre wavelength.

Chemotherapeutic agent kinetics. To elucidate drug-induced shifting (Fig. 1), a solution of 5 mg l^{-1} of GT–CoMoCAT SWNTs in 100 mM Tris buffer (pH 7.4) was exposed to 20 mM mechlorethamine, and spectra were acquired at room temperature. For kinetic measurements, 5 mg l^{-1} of GT–HiPCO in 100 mM Tris buffer (pH 7.4) was exposed to the alkylating agent melphalan, mechlorethamine or cisplatin at a concentration of 0.5 mM. Photoluminescence spectra were taken over 400–600 min at 37 °C. Unbound oligonucleotide kinetics were measured using polyacrylamide gel electrophoresis (PAGE) on the test sequence: 5′-TTT TTG TTT T-3′. The sequence was labelled with ^{32}P at the 5′ end and exposed to 0.5 mM of alkylating agent in 100 mM Tris (pH 7.5) at 37 °C. Aliquots were removed at each time point and held at −80 °C before 20% PAGE.

Reactive oxygen species. Transient photoluminescence measurements were conducted by exposing GT–CoMoCAT SWNTs in 20 mM Tris (pH 7.3) and 0.1 M NaCl (henceforth 'buffer') to 10 mM H_2O_2 in the case of H_2O_2 experiments. Singlet oxygen was induced with 0.1 mM $CuCl_2$ and 10 mM H_2O_2; hydroxyl radicals with 0.05 mM $FeSO_4$ and 10 mM H_2O_2. Cations were added to DNA–SWNT in buffer 1 h before the addition of H_2O_2 to rule out cation-induced effects[32]. Spectra were acquired over 10–400 min. Photoluminescence three-dimensional profiles were taken using 5 mg l^{-1} GT–CoMoCAT SWNTs in buffer with $CuCl_2$. The second profile was taken 24 h after exposure to 3.6 mM H_2O_2. All ROS experiments were conducted at room temperature.

Reactive oxygen species measurements after cation chelation. Solutions of 5 mg l^{-1} of GT–CoMoCAT SWNTs in buffer plus 0.1 mM $CuCl_2$ or 0.1 mM $FeSO_4$ and 2 mM EDTA were made before reacting with 1 mM H_2O_2. Photoluminescence measurements were taken 24 h later.

Reactive oxygen species measurements using different DNA sequences/cations. Solutions of 5 mg l^{-1} HiPCO SWNTs encapsulated by five different DNA sequences were made using the bath sonication method described above. Sequences were $d(T)_{30}$, $d(GGTT)_7TT$, $d(GAT)_{10}$, $d(GGGGT)_6$ and an oligonucleotide denoted Seq 1 containing the 27-nucleotide sequence 5′-ACC TGG GGG AGT ATT GCG GAG GAA GTT-3′ (purinic content = 67%). All other sequences were 30 nucleotides long. The photoluminescence of each sequence was measured upon reaction with 0.1 mM $CuCl_2$ and 3.6 mM H_2O_2 in buffer. The photoluminescence of GT–HiPCO was measured 24 h after reaction of 0.1 mM of various metallic cations with 3.6 mM H_2O_2 after 24 h to determine cation dependence on shift.

Cell culture. Murine NIH/3T3 cells were cultured with HEPES-buffered Dulbecco's Minimal Essential Media (DMEM, Sigma) supplemented with 10% fetal bovine serum (FBS, Biomeda). The cells were incubated with 2 mg l^{-1} of GT–CoMoCAT SWNT for 6–8 h before trypsin digestion and transfer to a separate container. Cells were plated on glass-bottomed petri dishes (MatTek) for microscopy.

Lysosomal imaging and photoluminescence/visible overlays. Lysosomal dye co-localization images were taken 2 h after exposing cells containing GT–CoMoCAT SWNTs to 70 nM of LysoTracker Red (Invitrogen). Cells were alternately exposed to white light excitation passed through a rhodamine dye filter cube for dye excitation and a 785 nm laser for SWNT imaging. Nanotube photoluminescence overlays on visible cell images were acquired by exposing the cells alternately to halogen epi-illumination and 785 nm excitation with detection by 2D InGaAs camera.

Live cell drug/reactive oxygen species perfusion. Cells adhering to glass-bottomed Petri dishes were imaged inside a micro-incubation platform (Model DH-40i, Warner Instruments). Alkylating drugs and other reagents were perfused by syringe. Cells were bathed in media with FBS during chemotherapeutics experiments. Mechlorethamine dissolved in DMEM media with FBS was perfused to reach a final concentration of 50 mM. Media were exchanged for saline solution just before ROS experiments to prevent cation precipitation and H_2O_2 degradation. The salts $CuCl_2$ or $FeSO_4$ were perfused approximately 30 min before measurements at 1 and 0.1 mM, respectively, and 30 mM H_2O_2 was perfused during data acquisition. Laser power was limited to 1.1 mW.

Principle components analysis. The analysis was conducted on all available sensor data assembled into a matrix of four columns, one for each of four X*i* measurements: (6,5) SWNT photoluminescence band energy and intensity, and (7,5) band energy and intensity. Early data points (zero concentration and zero time) were removed to clarify the plots, although their inclusion had negligible effect on the PCA. The first and second principal components, representing 89% of the variance of the sample, were PC1 = 0.9572X1 + 0.1073X2 + 0.2274X3 + 0.1433X4 and PC2 = −0.2729X1 + 0.4367X2 + 0.5071X3 + 0.6911X4.

Received 26 August 2008; accepted 13 October 2008; published online 14 December 2008

References

1. Barone, P. W., Baik, S., Heller, D. A. & Strano, M. S. Near-infrared optical sensors based on single-walled carbon nanotubes. *Nature Mater.* **4,** 86–92 (2005).
2. Saito, R., Dresselhaus, G. & Dresselhaus, M. S. *Physical Properties of Carbon Nanotubes* (Imperial College Press, 1998).
3. Heller, D. A. *et al.* Optical detection of DNA conformational polymorphism on single-walled carbon nanotubes. *Science* **311,** 508–511 (2006).
4. O'Connell, M. J. *et al.* Band gap fluorescence from individual single-walled carbon nanotubes. *Science* **297,** 593–596 (2002).
5. Lefebvre, J., Austing, D. G., Bond, J. & Finnie, P. Photoluminescence imaging of suspended single-walled carbon nanotubes. *Nano Lett.* **6,** 1603–1608 (2006).
6. Cognet, L. *et al.* Stepwise quenching of exciton fluorescence in carbon nanotubes by single-molecule reactions. *Science* **316,** 1465–1468 (2007).
7. Dukovic, G. *et al.* Reversible surface oxidation and efficient luminescence quenching in semiconductor single-wall carbon nanotubes. *J. Am. Chem. Soc.* **126,** 15269–15276 (2004).
8. Choi, J. H. & Strano, M. S. Solvatochromism in single-walled carbon nanotubes. *Appl. Phys. Lett.* **90,** 223114 (2007).
9. Rhee, S. G. H_2O_2, a necessary evil for cell signaling. *Science* **312,** 1882–1883 (2006).
10. Povirk, L. F. & Shuker, D. E. DNA damage and mutagenesis induced by nitrogen mustards. *Mutat. Res. Rev. Genet.* **318,** 205–226 (1994).
11. Delalande, O., Malina, J., Brabec, V. & Kozelka, J. Chiral differentiation of DNA adducts formed by enantiomeric analogues of antitumor cisplatin is sequence-dependent. *Biophys. J.* **88,** 4159–4169 (2005).
12. Tilby, M. J. *et al.* A monofunctional derivative of melphalan: Preparation, DNA alkylation products and determination of the specificity of monoclonal antibodies that recognize melphalan–DNA adducts. *Chem. Res. Toxicol.* **11,** 1162–1168 (1998).
13. Lovell, M. A. & Markesbery, W. R. Ratio of 8-hydroxyguanine in intact DNA to free 8-hydroxyguanine is increased in Alzheimer disease ventricular cerebrospinal fluid. *Arch. Neurol.* **58,** 392–396 (2001).
14. Hamilton, M. L. *et al.* Does oxidative damage to DNA increase with age? *Proc. Natl Acad. Sci. USA* **98,** 10469–10474 (2001).
15. Kawanishi, S., Hiraku, Y., Murata, M. & Oikawa, S. The role of metals in site-specific DNA damage with reference to carcinogenesis. *Free Radic. Biol. Med.* **32,** 822–832 (2002).
16. Imlay, J. A. Pathways of oxidative damage. *Annu. Rev. Microbiol.* **57,** 395–418 (2003).
17. Aruoma, O. I., Halliwell, B., Gajewski, E. & Dizdaroglu, M. Copper-ion-dependent damage to the bases in DNA in the presence of hydrogen peroxide. *Biochem. J.* **273,** 601–604 (1991).
18. Zheng, M. *et al.* DNA-assisted dispersion and separation of carbon nanotubes. *Nature Mater.* **2,** 338–342 (2003).
19. Jackson, E. J. *A User's Guide to Principal Components* (John Wiley & Sons, 2003).
20. Song, C. H., Pehrsson, P. E. & Zhao, W. Recoverable solution reaction of HiPco carbon nanotubes with hydrogen peroxide. *J. Phys. Chem. B* **109,** 21634–21639 (2005).
21. Tu, X. M., Pehrsson, P. E. & Zhao, W. Redox reaction of DNA-encased HiPCO carbon nanotubes with hydrogen peroxide: A near infrared optical sensitivity and kinetics study. *J. Phys. Chem. C* **111,** 17227–17231 (2007).
22. Burrows, C. J. & Muller, J. G. Oxidative nucleobase modifications leading to strand scission. *Chem. Rev.* **98,** 1109–1151 (1998).
23. Duguid, J., Bloomfield, V. A., Benevides, J. & Thomas, G. J. Raman spectroscopy of DNA-metal complexes. 1. Interactions and conformational effects of the divalent-cations — Mg, Ca, Sr, Ba, Mn, Co, Ni, Cu, Pd and Cd. *Biophys. J.* **65,** 1916–1928 (1993).
24. Lloyd, D. R. & Phillips, D. H. Oxidative DNA damage mediated by copper(II), iron(II) and nickel(II) Fenton reactions: evidence for site-specific mechanisms in the formation of double-strand breaks, 8-hydroxydeoxyguanosine and putative intrastrand cross-links. *Mutat. Res. Fund. Mol. M.* **424,** 23–36 (1999).
25. Yang, J. L., Wang, L. C., Chang, C. Y. & Liu, T. Y. Singlet oxygen is the major species participating in the induction of DNA strand breakage and 8-hydroxydeoxyguanosine adduct by lead acetate. *Environ. Mol. Mutagen.* **33,** 194–201 (1999).
26. Kerssemakers, J. W. J. *et al.* Assembly dynamics of microtubules at molecular resolution. *Nature* **442,** 709–712 (2006).
27. Kam, N. W. S., O'Connell, M., Wisdom, J. A. & Dai, H. J. Carbon nanotubes as multifunctional biological transporters and near-infrared agents for selective cancer cell destruction. *Proc. Natl Acad. Sci. USA* **102,** 11600–11605 (2005).
28. Cherukuri, P., Bachilo, S. M., Litovsky, S. H. & Weisman, R. B. Near-infrared fluorescence microscopy of single-walled carbon nanotubes in phagocytic cells. *J. Am. Chem. Soc.* **126,** 15638–15639 (2004).
29. Heller, D. A., Baik, S., Eurell, T. E. & Strano, M. S. Single-walled carbon nanotube spectroscopy in live cells: Towards long-term labels and optical sensors. *Adv. Mater.* **17,** 2793–2799 (2005).
30. Gaetani, G. F. *et al.* Predominant role of catalase in the disposal of hydrogen peroxide within human erythrocytes. *Blood* **87,** 1595–1599 (1996).
31. Jin, H., Heller, D. A. & Strano, M. S. Single-particle tracking of endocytosis and exocytosis of single-walled carbon nanotubes in NIH-3T3 cells. *Nano Lett.* **8,** 1577–1585 (2008).
32. Jin, H. *et al.* Divalent ion and thermally induced DNA conformational polymorphism on single-walled carbon nanotubes. *Macromolecules* **40,** 6731–6739 (2007).

Acknowledgements

M.S.S is grateful for a Beckman Young Investigator Award and a National Science Foundation (NSF) Career Award. This work was funded under the NSF Nanoscale Interdisciplinary Research Team on single molecule detection in living cells using carbon nanotube optical probes. The authors thank S. McMasters (University of Illinois) for cell culture assistance, and C. Fantini, A. Jain, A. Moll and J. Ossyra for experimental assistance. We also thank S. Tannenbaum, G. Wogan and L. Trudel and acknowledge a seed grant from the Center for Environmental Health Sciences at MIT. Partial support was provided by the National Cancer Institute (U54-CA119342-01) to the Siteman Center of Cancer Nanotechnology Excellence, through the University of Illinois Center for Nanoscale Science and Technology.

Author contributions

D.H. and M.S. originated the concept for the paper and the experimental validation. D.H., H.J., B.M., D.P., B.M., T.-K.Y., P.J. and C.H. all assisted in the experiments. D.H., B.M., D.P., B.M., T.-K.Y., P.J. and C.H. performed the data analysis. S.S., T.H., C.H. and P.J. contributed materials/specific analysis tools and provided useful discussions. D.H. and M.S. co-wrote the paper with input from S.S.

Additional information

Supplementary Information accompanies this paper at www.nature.com/naturenanotechnology. Reprints and permission information is available online at http://npg.nature.com/reprintsandpermissions/. Correspondence and requests for materials should be addressed to M.S.S.